LARGE EDDY SIMULATION OF COMPRESSIBLE TURBULENT MIXING

Ben Thornber*, Andrew Mosedale & Dimitris Drikakis
Fluid Mechanics and Computational Science Group
Department of Aerospace Sciences
Cranfield University
MK43 0AL
UK
* b.j.r.thornber@cranfield.ac.uk

ABSTRACT

This paper presents implicit large eddy simulation of compressible turbulent mixing produced by a shock wave passing through a perturbed gas interface. Two different initial conditions are employed, three different grid sizes for each initial condition, and two very high order numerical methods. Solutions are gained which are reasonably grid converged, and approach a quasi self-similar state. It is shown that the choice of initial conditions affect significantly the growth of the turbulent mixing zone, and the plane averaged mixing parameters. The high wavenumber initial perturbation leads to a smoother mean volume fraction profile, and a lower growth rate. Employing low wavenumber perturbations gives a faster growth rate due to the presence of long wavelengths which grow on a longer timescale. The paper discusses further the behaviour of resolved turbulent kinetic energy, kinetic energy spectra, and self-similarity of plane averaged quantities.

INTRODUCTION

This paper concerns large eddy simulations (LES) of shock wave induced instabilities (Richtmyer-Meshkov) and turbulent mixing. Richtmyer Meshkov (RM) (Richtmyer, 1960) instability occcurs when an incident shock wave passes through a perturbed interface between two gases, triggering growth of the interface width. These instabilities first grow linearly, and then transition to turbulence. They are of importance in the study of supernovae explosions, wakes of jet engines, combustion chambers and inertial confinement fusion.

In engineering analysis often it is assumed that initial conditions are forgotten, and hence are not important to the late time development of turbulence. However, in nature the initial perturbations are formed as a summation of unstable modes which each grow at different rate. It has been demonstrated that the form of the initial perturbations can affect significantly the growth of the resulting mixing layer in idealised Rayleigh Taylor, Kelvin Helmholtz and Richtmyer-Meshkov instabilities (Youngs,2004). This is due to the finite time taken to redistribute the kinetic energy deposited by the shock wave between the turbulent components, where anisotropy potentially can persist over a long period of time.

This paper investigates the growth of a Richtmyer-Meshkov mixing layer using two different perturbations. The first is a narrowband combination of high frequency modes, which represents growth of a turbulent mixing layer purely via mode coupling of the high wave numbers. The second initial condition consists of a broadband linear combination of modes from one third the domain size to the high frequencies. If the initial conditions are forgotten then the asymptotic growth rate, and associated statistics of the mixing layer should be the same in both cases. However, it is possible that the large scale perturbations continue growing to a later time, hence dominating the growth of the turbulent mixing zone.

As current computational power does not allow Direct Numerical Simulation of such complex flows, Large-eddy simulation (LES) is as a viable alternative in flows of industrial interest where the time dependent behaviour of the flow must be resolved. Conventional LES, where an explicit subgrid model is added to the averaged Navier Stokes equations, has been employed successfully in many prototype flows, however it is known to provide excessive dissipation in flows where the growth of an initially small perturbation to fully turbulent flow must be resolved. It has been recognised that some numerical schemes, labelled as high-resolution methods, gain good results in complex flows without the explicit addition of a subgrid model (Lesieur and Metais, 1996). This approach is termed Implicit Large-eddy Simulation, or ILES. This paper employs three different variable reconstruction methods: second-order van Leer limiting; ninth-order WENO (Balsara,2000); and a recently developed fifth-order MUSCL scheme (Thornber,submitted).

NUMERICAL METHODS

Governing Equations

This paper is concerned with the simulation of the Euler equations, where viscosity is assumed negligible ($Re \rightarrow \infty$). The three-dimensional compressible Euler equations are solved using the direction split method. This involves solving in each principal direction the following governing equations,

$$\frac{\partial \mathbf{U}}{\partial t} + \frac{\partial \mathbf{E}}{\partial x} = 0, \tag{1}$$

where,

$$\mathbf{U} = \left[\rho,\ \rho u,\ \rho v,\ \rho w,\ e\right]^T, \tag{2}$$

$$\mathbf{E} = \left[\rho u,\ \rho u^2 + p,\ \rho uv,\ \rho uw,\ (e+p)u\right]^T, \tag{3}$$

$$e = \rho i + 0.5\rho\left(u^2 + v^2 + w^2\right), \tag{4}$$

and ρ, i, u, v, w are the density, specific internal energy per unit volume and Cartesian velocity components, respectively. Throughout this paper it is assumed that the fluid satisfies the ideal gas equation of state

$$p = \rho i\left(\gamma - 1\right), \tag{5}$$

where $\gamma = 5/3$ is the ratio of specific heats. In addition, a passive scalar is advected to track the two gas components, assumed to be miscible.

Numerical Methods

The numerical method is a standard finite volume solver employing the HLLC approximate Riemann solver (Toro,1997). Higher order accuracy is achieved using MUSCL extrapolation,

$$\mathbf{P}^L_{i+1/2} = \mathbf{P}_i + \frac{1}{2}\phi\left(r^L\right)\left(\mathbf{P}_i - \mathbf{P}_{i-1}\right) \quad (6)$$

$$\mathbf{P}^R_{i+1/2} = \mathbf{P}_{i+1} - \frac{1}{2}\phi\left(r^R\right)\left(\mathbf{P}_{i+2} - \mathbf{P}_{i+1}\right) \quad (7)$$

where $\mathbf{P}$ is the vector of cell averaged primitive variables, and the cells are labelled by the integer i. Also,

$$r^L_i = \frac{\mathbf{P}_{i+1} - \mathbf{P}_i}{\mathbf{P}_i - \mathbf{P}_{i-1}} \quad (8)$$

$$r^R_i = \frac{\mathbf{P}_{i+1} - \mathbf{P}_i}{\mathbf{P}_{i+2} - \mathbf{P}_i} \quad (9)$$

The third-order van Leer (van Leer,1977) and fifth-order limiters (Kim and Kim,2005) are employed

$$\phi_{VL} = \frac{2r}{1+r} \quad (10)$$

$$\phi_{L,M5} = \frac{-2/r^L_{i-1} + 11 + 24r^L_i - 3r^L_i r^L_{i+1}}{30} \quad (11)$$

$$\phi_{R,M5} = \frac{-2/r^R_{i+2} + 11 + 24r^R_{i+1} - 3r^R_{i+1} r^R_i}{30} \quad (12)$$

where monotonicity is maintained in the fifth-order method by limiting the above extrapolations using

$$\phi_{L,M5} = max(0, min(2, 2r^L_i, \phi_{5th,L})) \quad (13)$$

$$\phi_{R,M5} = max(0, min(2, 2r^R_i, \phi_{5th,R})) \quad (14)$$

This limiter has been modified to significantly improve performance in resolving fine scale motion, particularly at low Mach. It ensures that the dissipation rate is constant, and that pressure is coupled with the vorticity field as Mach tends to zero, without sacrificing the scheme's ability to capture shocks and explicit stability (Thornber,submitted). The modified scheme resolves modes to a higher wavenumber than standard ninth-order WENO and van Leer reconstruction methods.

The WENO ninth-order method employed is that by Balsara and Shu (2000), which uses a weighted combination of non-linear polynomials to achieve higher order accuracy with minimum impact on the monotonicity of the resulting schemes.

Initialisation

The test case uses the initial conditions derived by Youngs (2004) to examine the influence of initial conditions on the growth of the resultant mixing layer. The flowfield consists a heavy and light gas separated by a perturbed interface where the perturbation satisfies a given power spectrum and mean amplitude. The incident shock wave is of Mach= 1.84, equivalent to a four-fold pressure increase across the shock wave. The initial conditions are

$$0.0 < x < 2.3(\rho, u, p) = (6.38, -61.5, 4 \times 10^5) \quad (15)$$

$$2.3 < x < 3.35 + \xi(\rho, u, p) = (3.0, -291.58, 10^5) \quad (16)$$

$$3.35 + \xi < x < L_D(\rho, u, p) = (1.0, -291.58, 10^5) \quad (17)$$

where an initial velocity is given to the gas interface such that the centre of the interface is stationary after passage of the shock wave. The ratio of specific heats, γ, is set to 5/3.

For the broadband initialisation, the interface perturbation ξ is given as the sum of modes of random phase conforming to an initial power spectrum $P \propto c/k^2$. The modes excited are restricted between $\lambda_{min} = 32\pi/256$ and $\lambda_{max} = 2\pi/3$ and the standard deviation of the perturbation amplitude is $0.1\lambda_{min}$. The grid sizes used were $360 \times 256 \times 256$, $180 \times 128 \times 128$ and $90 \times 64 \times 64$, and the domain size is fixed at $2.4\pi \times 2\pi \times 2\pi$. This is essentially a convergence study with the same initial condition on all grids, only more poorly resolved on the coarsest grid. This problem was solved with the modified fifth-order limiter for all grids, and the WENO ninth-order for the coarse and medium grids.

The narrowband perturbation has an initial power spectrum $P \propto c$, and excited modes lie between $\lambda_{min} = 16\Delta x$ and $\lambda_{max} = 32\Delta x$. The initial amplitude is $0.1\lambda_{min}$. In this case the initial perturbation has been chosen to lie at a high frequency, but where the numerical scheme resolves perturbations without dampening. This problem employs grids of size $360 \times 300 \times 300$, $360 \times 150 \times 150$ and $360 \times 75 \times 75$. As the initial perturbation and amplitude is linked to the grid scale, the perturbations on the smaller grid grow faster, proportional to λ_min. To compensate for this the grid size in the x-direction is increased proportionally such that the mesh remains square at all resolutions. In order of decreasing mesh size, the domain sizes are; $2.4\pi \times 2\pi \times 2\pi$, $4.8\pi \times 2\pi \times 2\pi$ and $9.6\pi \times 2\pi \times 2\pi$. This problem was solved using the modified fifth-order limiter.

RESULTS AND DISCUSSION

Non-Dimensionalisations

Before discussing the results, it is important to set out the relevant scaling laws and non-dimensionalisations. Following Youngs (1994) all lengthscales are normalised by the minimum wavelength λ_{min}, and wave numbers by $k_{min} = 1/\lambda min$. The time is scaled via λ_{min} and Δu, which is the velocity impulse given to the interface. Finally, total Kinetic Energy, and the kinetic energy spectra are non-dimensionalised by $\lambda_{min}\Delta u^2 \rho$, where $\rho = 1$. All subsequent results are non-dimensional.

Note that in all subsequent figures the standard numerical scheme is the modified fifth order method.

Flow Phenomenology

Figure 1 shows mass fraction isosurfaces illustrating the initial condition and evolution of the turbulent interface with time. It can be seen that for early time ($t\Delta u/\lambda_{min} = 7$) the flow field consists of a series of mushroom like structures generated by the deposition of vorticity at the gas interface. Kelvin-Helmoltz (KH) instabilities grow exponentially hence breaking the large coherent structures. At late time the flow field is turbulent, consisting of motion on many different scales. There are some 'coherent' structures remaining

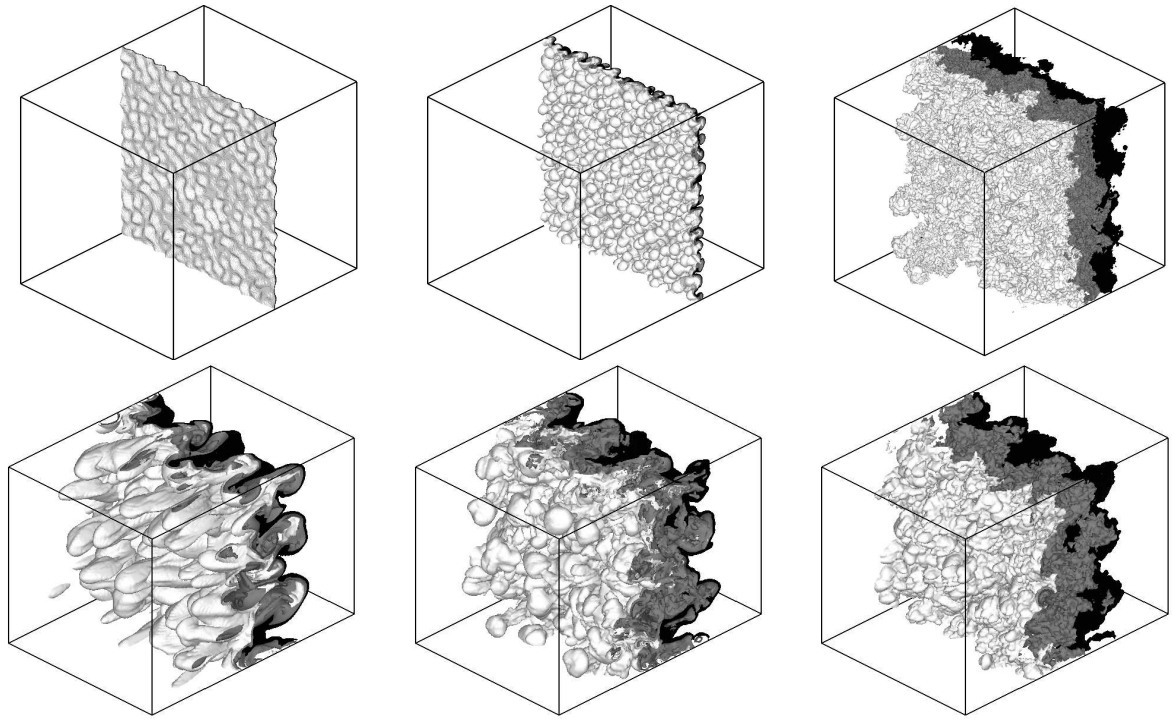

Figure 1: Evolution of mass fraction isosurfaces for the fine grid narrowband perturbations at $t\Delta u/\lambda_{min} = 0$, 7 and 250 using the modified fifth order scheme (top) and a comparision of the three numerical methods using broadband perturbations at $t\Delta u/\lambda_{min} = 250$ at 128 grid cross-section (bottom)

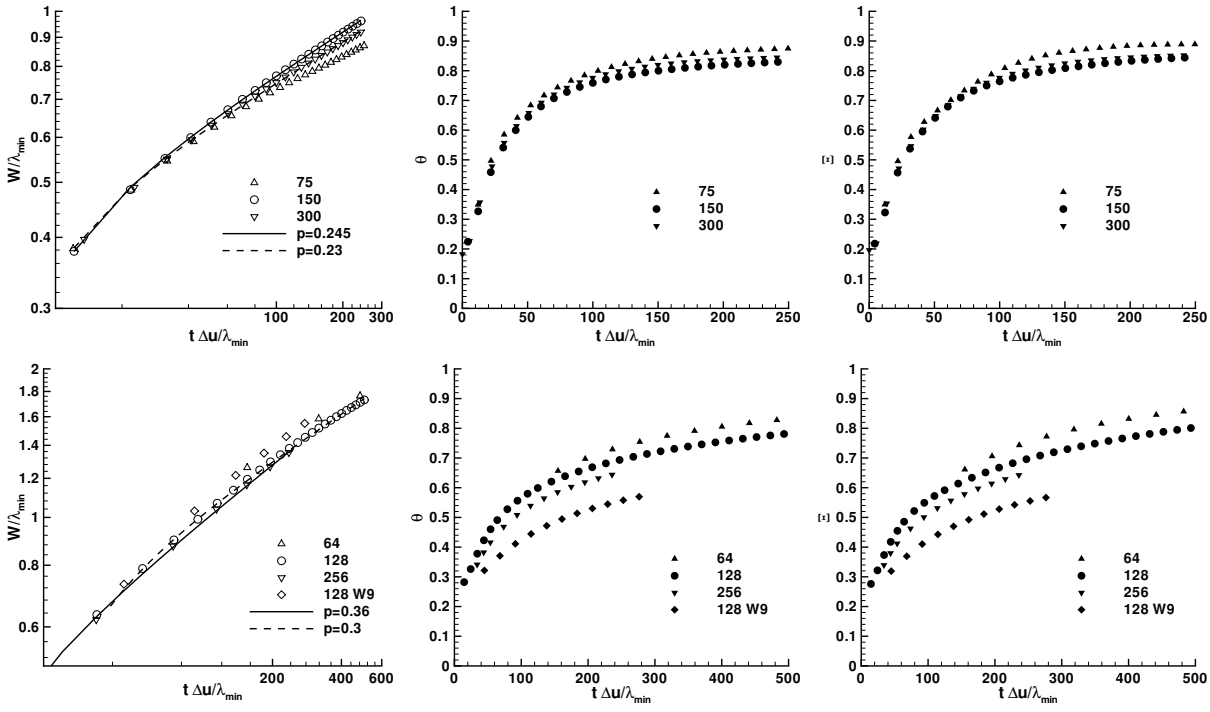

Figure 2: Integral mixing width, Molecular mixing fraction and mixing parameter for the narrowband perturbations (top) and broadband (bottom)

(mushrooms shedding KH vortices) at the gas front, but in-between there is a well mixed zone.

Figure 1 also shows the isosurfaces of mass fraction for each of the three numerical methods at late time for the 128 cross-section grid (broadband initial conditions). It is clear that the van Leer limiter is too dissipative to allow realistic growth of perturbations, hence, to economise on space, further results are not presented here. Of WENO ninth order (W9) and the modified fifth order (M5) the fifth-order has more fine scale structure, indicating less numerical dissipation.

Growth Rates and Mixing Measures

Linear theory dictates that the rate of growth of the mixing layer V is proportional to $k\Delta v a_0 A$, where k is the wavenumber, Δv the velocity impulse, a_0 the initial amplitude of the wave and $A = (\rho_2 = \rho_1)/(\rho_1 + \rho_2)$, the Atwood number. In this section the following parameters are examined; Integral mixing layer width $W = \int f_1 f_2 dx$; Molecular mixing fraction $\theta = \int < f_1 f_2 > dx / \int < f_1 >< f_2 > dx$; and the mixing parameter $\Xi = \int < min(f_1, f_2) > dx / \int min(< f_1 >, < f_2 >) dx$. $< f_a >$ indicates the $y-z$ plane averaged volume fraction of species a, where species 1 is the heavy gas. It is generally accepted that the integral mixing layer width, defined as $W = \int f_1 f_2 dx$ (considered less sensitive to fluctuations) grows at late time as t^p. θ gives a guide to the total reaction rate for a slow reaction, and Ξ is an equivalent measure for a fast reaction rate where one reactant is fully depleted.

Figure 2 shows these quantities plotted for both sets of initial conditions, for all grid resolutions. The mixing layer width exhibits good grid convergence, and is plotted on logarithmic axes to highlight the power-law behaviour of the amplitude. Assuming that amplitude is proportional to t^p, giving $p = 0.24 \pm 0.015$ for the narrowband simulation, and $p = 0.33 \pm 0.03$ for the broadband initial conditions. This demonstrates that, for the duration of the simulation, the mixing layer width depends crucially on the form of the initial conditions.

The molecular mixing fraction θ and mixing parameter Ξ both approach a constant state. This is achieved more rapidly with narrowband perturbations than with the broadband initialisation. At the lower resolutions with M5 the level of molecular mixing is higher than with the WENO method, however as grid size increases both θ and Ξ decrease. The asymptotic value of approximately 0.8 agrees well with previous mixing simulations of the related Rayleigh-Taylor instability by Youngs (2003) and Cook and Zhou (2002). The slower convergence of the mixing statistics at high grid resolution indicates that a self-similar state has not yet been achieved for the broadband simulations.

For self-similarity the profiles of average volume fraction and mixing fractions should scale with a single characteristic lengthscale at all times, in this case the integral mixing layer width W. Figure 3 shows the plane averaged volume fraction, and Figure 4 the plane averaged mixing fraction $< f_1 f_2 >$. The scaled volume fraction profiles collapse excellently for all resolutions at all times for the narrowband and broadband perturbations, being almost identical at all times.

The narrow band perturbations lead to a smoother mean volume fraction profile, whereas the broad band perturbations give a smooth central region ($-1.5 < x/W < 1.5$) with outer regions on the bubble and spike side where the persisting large scale structures cause a break in the smooth

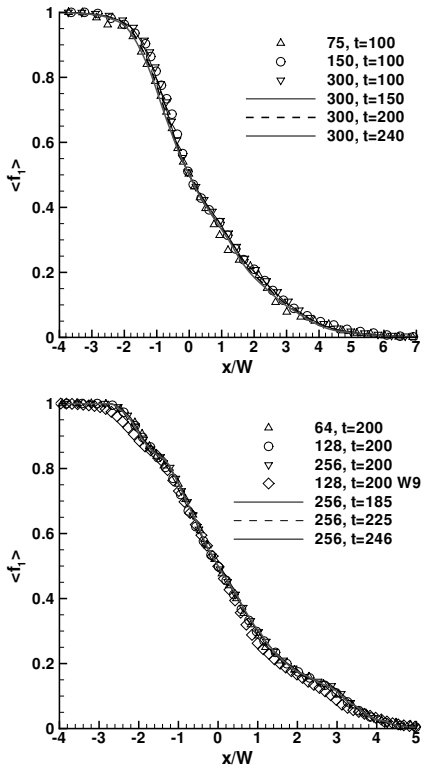

Figure 3: Plane averaged volume fraction for narrowband (top) and broadband (bottom) perturbations.

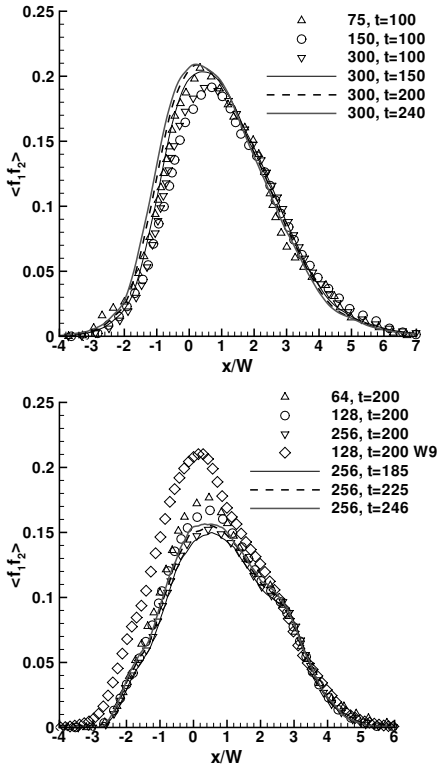

Figure 4: Plane averaged mixing fraction for narrowband (top) and broadband (bottom) perturbations.

profile. This change to the mean profile is most likely the late time growth of large scale perturbations which are not present in the narrowband simulation, and are at the head and tail of the mixing layer at late times.

The plane averaged mixing fractions are not as well converged. Interestingly, the level of mixing appears to be decreasing at higher resolution in both cases, indicating that the lower dissipation at higher resolution leads to less diffusive transport. The WENO limiter promotes greater mixing, having a profile which peaks at $< f_1 f_2 >= 0.21$ as opposed to 0.16 for the M5 limiter at the same resolution. As time progresses the peak of $< f_1 f_2 >$ increases, as expected.

Turbulent Kinetic Energy

Figure 5 shows the total fluctuating kinetic energy (point value in the x and y direction respectively, the z omitted as it is very similar to the y direction. This is computed from the fluctuating velocities, i.e. the point velocities minus the plane average velocities. Additionally, the instantaeneous two dimensional kinetic energy spectra is plotted for the centre of the mixing layer in the homogeneous $y - z$ plane.

Both simulations demonstrate excellent grid convergence, the x direction turbulent kinetic energy decreasing throughout the simulations in a power law form. The y and z direction kinetic energy first increases as KH instability transfers energy from the x direction to the y and z. In the narrowband simulation the turbulent kinetic energy in the x direction decreases at a rate proportional to $t^{-1.24}$, in the y and z proportional to $t^{-1.2}$, in good agreement with experimental results from grid generated homogeneous decaying turbulence (Kang,2002). This is also seen at 128 and 256 resolution in the broadband initial condition, but with a decay rate proportional to $t^{-1.05}$ for the x direction turbulent kinetic energy, and $t^{-0.8}$ for the y and z directions. It appears that both initialisations are tending towards a homogeneous state as time progresses.

The two dimensional kinetic energy spectra are compared to the theoretical results of Kolmogorov ($k^{-5/3}$) and the proposed solution for RM instability of $k^{-3/2}$ by Zhou (Zhou,2001). This is computed in the midplane of the mixing layer, in the $y - z$ plane. Examining the narrowband results indicates excellent scaling of the kinetic energy spectra from the different grid resolutions under the non-dimensionalisations detailed in Section . The small scales are nearly identical, and the spectra appear to follow more closely the $k^{3/2}$ spectrum. The differences at large scales (low wavenumbers) reflect the limitations posed by grid size, which prevents further mode coupling in the low resolution simulations.

The broadband spectra also collapse well at different grid resolutions, and methods. Comparison between the different grids and methods show that the M5 method is not sufficiently dissipative at low resolutions, and that the WENO method is too dissipative. This is consistent with the plane averaged mixing results presented in Figure 4, which demonstrate more mixing at the lower resolutions than at the higher resolutions. At the highest resolutions there is excellent agreement for the first 48 modes when comparing the 128 and 256 cross-section grids with the M5 method, and up to mode 28 with WENO. At moderate wavenumber the spectra appear to scale as $k^{-5/3}$, and at $k^{-3/2}$ at high wavenumber.

CONCLUSIONS

Simulations of shock induced turbulent mixing with two different initial conditions have been conducted. Two different high order methods have been used, and three different grid sizes. Excellent grid convergence is observed throughout.

The typical behaviour of a multimode Richtmyer-Meshkov simulation is seen, beginning with the growth of coherent 'mushroom' shaped structures which transition to a fully turbulent mixing zone. It is shown that the growth rate of the mixing zone depends on the initial perturbation, as the long wavelength perturbations promote a faster growth rate than short wavelength perturbations. This is most likely to be due to the slow but persistent growth of large scale perturbations which dominate over the short wavelengths at long times. Examining the mean volume fraction profiles and development of two mixing indicators implies that the development of the mixing zone has reached an approximate self-similar state. The asymptotic state is not reached as rapidly for the broadband perturbations as for the narrowband.

The turbulent kinetic energy decays more rapidly in the narrow band simulation, close to that expected from homogeneous decaying turbulence. However, the broadband simulation demonstrates slower decay. In both simulations the turbulent kinetic energy components are tending towards isotropy, but do not reach it in the time range simulated. Turbulent kinetic energy spectra show a closer agreement to a $k^{-3/2}$ range at the high wavenumbers, with some $k^{-5/3}$ at intermediate scales.

ACKNOWLEDGEMENTS

The authors would also like to acknowledge assitance and advice from David Youngs and Robin Williams both at AWE, Aldermaston. They would also like to acknowledge financial support through an EPSRC-AWE PhD CASE award and an EPSRC-MoD (Dstl, AWE) research grant (EP/C515153 & JGS 971).

REFERENCES

Balsara, D. and Shu, C-W., 2000, "Monotonicity preserving weighted essentially non-oscillatory schemes with increasingly high order of accuracy", *J. Comput. Phys.*, Vol. 160, pp. 405-452

Cook, A.W. and Zhou, Y., 2002, "Energy Transfer in Rayleigh-Taylor Instability", *Phys. Rev. E*, Vol. 66, 026312

Kim, K.H. and Kim, C., 2005, "Accurate, efficient and monotonic numerical methods for multi-dimensional compressible flows Part II: Multi-dimensional limiting process", *J. Comput. Phys.*,Vol. 208, pp. 570-615

Lesieur, M. and Metais, O., 1996, "New trends in large-eddy simulations of turbulence",*Annu. Rev. Fluid Mech.*, Vol. 28, pp. 45-82

Richtmyer, R.D., 1960, "Taylor instability in shock acceleration of compressible fluids",*Comm. Pure Appl. Math.*, Vol. 13, pp. 297–319

Toro, E., 1997, "Riemann solvers and numerical methods for fluid dynamics", Springer-Verlag

Thornber, B., Mosedale, A. Drikakis, D., and Youngs, D., "The dissipation of kinetic energy within Godunov schemes II: Numerical Modification", *submitted to J. Comput. Phys.*

van Leer, B., 1977, "Towards the ultimate conservative difference scheme.IV. A new approach to numerical convection", *J. Comput. Phys.*, Vol. 23, pp. 276-299

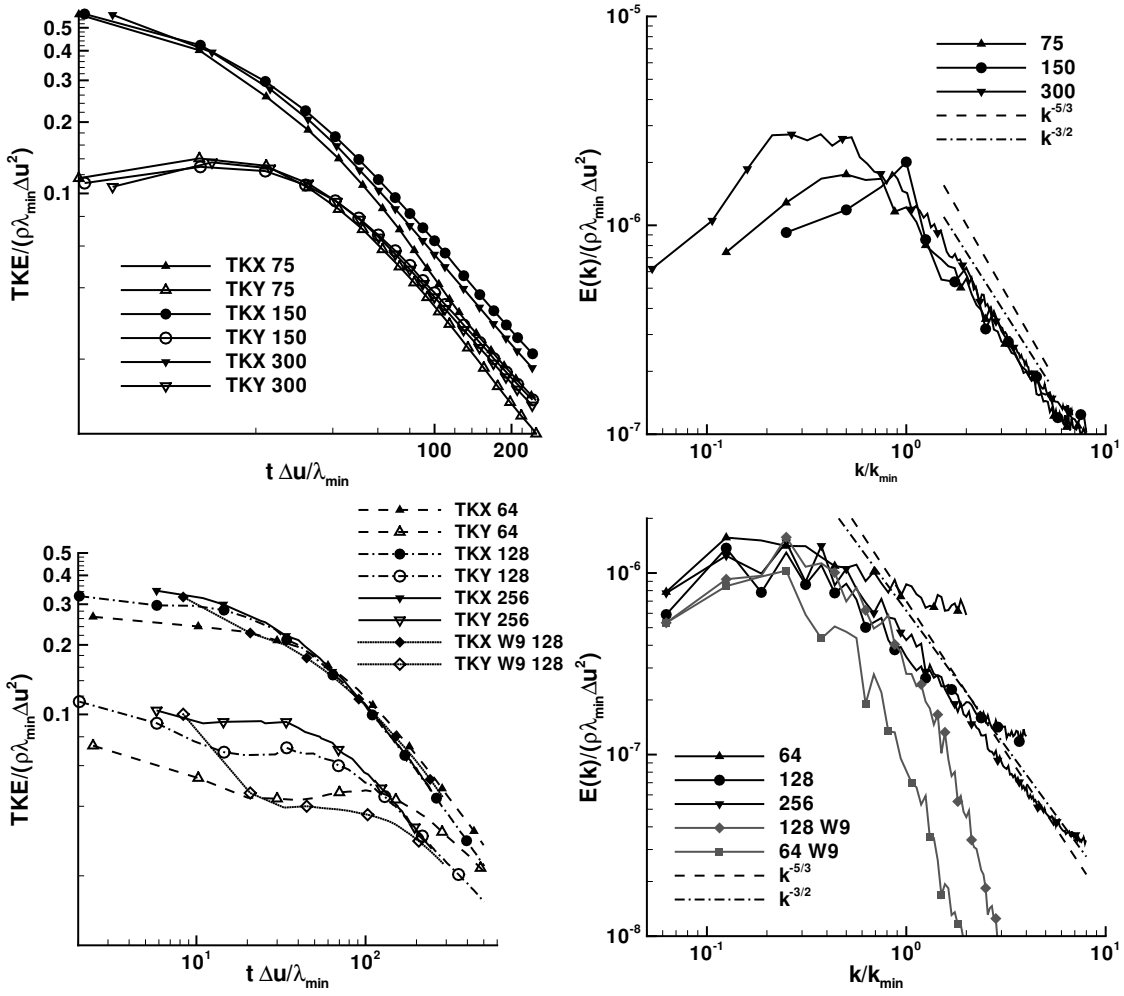

Figure 5: Resolved fluctuating kinetic energy and kinetic energy spectra for the narrowband (top) and broadband case (bottom)

Youngs, D.L., 1994, "Numerical simulation of mixing by Rayleigh-Taylor and Richtmyer-Meshkov instabilities",*Laser Part. Beams*, Vol. 12, pp. 725-750

Youngs, D.L., 2003, "Application of MILES to Rayleigh-Taylor and Richtmyer-Meshkov Mixing" *AIAA*, AIAA-2003-4102

Youngs, D.L., 2004,"Effect of initial conditions on self-similar turbulent mixing",*Proceedings, IWPCTM 9*,2004

Zhou, Y., 2001, "A scaling analysis of turbulent flows driven by Rayleigh-Taylor and Richtmyer-Meshkov instabilities", *Phys. Fluids*, Vol. 13:2, pp. 538-543